ZnO-Al_2O_3 nanocomposite as a sensitive layer for high performance surface acoustic wave H_2S gas sensor with enhanced elastic loading effect

Yongliang Tang[1,*], Xiaofeng Xu[2], Shaobo Han[2], Chao Cai[2], Huarong Du[1], Hao Zhu[1], Xiaotao Zu[2], YongQing Fu[3]

[1]School of Physical Science and Technology, Southwest Jiaotong University, Chengdu, 610031, P. R. China

[2]School of Physics, University of Electronic Science and Technology of China, Chengdu, 610054, P. R. China

[3]Faculty of Engineering and Environment, Northumbria University, Newcastle upon Tyne, NE1 8ST, UK

[*]Correspondence Author:

Yongliang Tang: E-mail address: tyl@swjtu.edu.cn; Telephone: +86-15884573263

Abstract:

$ZnO\text{-}Al_2O_3$ nanocomposite was synthesized and developed as a high performance sensitive and selective layer for surface acoustic wave (SAW) sensor, aiming for *in-situ* detection of H_2S gas in ppb level operated at room temperature. $ZnO\text{-}Al_2O_3$ nanocomposite, synthesized though a sol-gel method, was spin-coated onto a quartz based SAW resonator. This composite layer inherits the mesoporous structure of the Al_2O_3 layer and good affinity to H_2S gas molecules of the ZnO layer, and thus can selectively adsorb and react with H_2S gas molecules to form ZnS compounds on its surface. This reaction leads to significant decreases of both pore sizes and total pore volume of the layer, an increase of layer's elastic modulus, thus causing a large positive shift of the frequency responses of the SAW sensor. The sensor operated at room temperature shows a frequency response of ~500 Hz to 10 ppb H_2S, with an excellent selectivity and good recovery property.

Key words: H_2S; Gas sensor; Surface acoustic wave; $ZnO\text{-}Al_2O_3$; Elastic modulus

1. Introduction

H_2S gas is neuro-toxin, and it can cause acute poisoning of a person in an hour when its concentration in the environment is higher than 100 ppm [1-4]. In addition, H_2S gas with a concentration higher than 500 ppm can lead to the sudden collapse and death of a person. H_2S with a relatively lower concentration than the above-mentioned ones can cause various chronic illnesses, such as obstructive pulmonary emphysema and chronic bronchitis, etc. [4-6]. Despite its hazard, H_2S gas is vastly used in various industrial fields, because it is among one of the important industrial chemicals for oil, water treatment and chemical industries [7-9]. Therefore, it is critical to develop sensitive, selective and reliable H_2S gas sensors for *in-situ* and precise monitoring of the concentration of H_2S gas in the environment.

Recently, surface acoustic wave (SAW) technique has been used in the H_2S gas sensing because of its advantages of low power consumption, low operation temperature, excellent stability, sensitivity and wireless control capabilities [10-13]. Semiconducting oxides such as SnO_2, CuO and WO_3 are usually employed as sensing layers of SAW based H_2S sensors. For example, Luo et al. [11] fabricated a SAW H_2S gas sensor based on a sol-gel SnO_2 layer and achieved a detection limit of 1.5 ppm. Wang et al. [14] prepared a SnO_2/CuO composite film for a SAW H_2S sensor and achieved a high sensitivity of 16.9 kHz/ppm. Galipeau et al. [15] reported a SAW H_2S sensor using WO_3 as the sensitive layer, and it achieved a response of ~600 Hz to 0.25 ppm H_2S. These studies [10-17] have all concluded that the key sensing mechanism of the sensors are the changes of the weight (mass loading effect) and electrical conductivity (electrical loading effect) of the sensing layers when the sensor is exposed to H_2S gas. However, as we know, there is another important sensing mechanism, i.e., the changes of elastic modulus (elastic loading effect), which has seldomly been

investigated or explored for H_2S gas sensing using the SAW technique. Nevertheless, this elastic loading effect could play an important role in the sensing performance of a SAW gas sensor based on semiconducting oxide based sensing layers [18-22]. For example, Raj et al. [22] reported that a SAW gas sensor coated with SnO_2 layer is a good NO_2 sensor as its elastic modulus changes significantly which significantly contributes the responses of the sensor.

In this research, we proposed a mesoporous ZnO-Al_2O_3 nanocomposite layer which can significantly enhance the elastic loading effect and thus increase the H_2S gas sensing performance of SAW sensors. This nanocomposite layer inherits the mesoporous structure of pristine Al_2O_3 layers, and previous studies [23-25] have revealed that ZnO has a high affinity to the H_2S molecules and can be used as a desulphurizer for the adsorption and removal of H_2S at room temperature. Therefore, ZnO component in the nanocomposite layer can act as the active capturing and adsorption sites for the H_2S gas. In addition, the adsorbed H_2S molecules can spontaneously react with the ZnO nanoparticles to form ZnS [26-29], which has a lower density and higher mole weight than those of the ZnO. Therefore, the formation of ZnS will result in decreases of pore sizes and total pore volumes in the layer, which lead to an increase of layer elastic modulus, thus resulting in a significant increase of sensor's response. Based on this enhanced elastic loading effect, the sensor with the mesoporous ZnO-Al_2O_3 composite layer has been successfully demonstrated to detect 10 ppb H_2S with a response of ~500 Hz.

2. Experimental details

Commercial ST-Cut quartz substrate was used for the fabrication of the SAW device. Aluminum interdigital transducers (IDTs, 30 pairs) and reflecting gratings (100 pairs) with a thickness of 200 nm were deposited on the substrate using standard photolithography and lift-off processes to build the SAW resonator. The IDTs and reflecting gratings have a periodicity of 16 μm, thus the designed operating frequency of the resonator is ~200 MHz. The center-to-center distance between the IDTs is 230 wavelengths.

The sensing layers were deposited onto the SAW resonator using a method combining sol-gel and spin-coating techniques. ZnO sol was prepared using a technique reported in our previous paper [30]. Typically, zinc acetate dehydrate ($Zn(CH_3COO)_2 \cdot 2H_2O$) was dissolved into a 2-methoxyethanol monoethanolamine (MEA) solution. The molar ratio of the MEA to zinc acetate was maintained at 1.0, and the concentration of the zinc acetate was 0.3 mol/L. The resultant solution was stirred at 60 ^oC for 1 hour to produce a clear and homogeneous solution, which was then aged for 1 day to obtain the ZnO sol. For preparation of Al_2O_3 sol, aluminum tri-sec-butoxide was firstly added into ethanol in a beaker under continually magnetic stirring at room temperature. The obtained mixture was stirred for two hours to obtain a homogeneous solution. Then appropriate amount of water was added into the solution to catalyze the hydrolysis of aluminium tri-sec-butoxide. As a result, a creamy white sol was obtained. Nitric acid was added inside the creamy white sol, and a clear colloid sol with a concentration of 0.3 mol/L was finally obtained. For the preparation of ZnO-Al_2O_3 mixture sol, the two colloidal sols were mixed in a beaker with Zn/Al molar ratio of 1:1, and the obtained precursor solution was stirred at 30 ^oC for two hours and aged for 1 day to obtain ZnO-Al_2O_3 colloidal sols.

The obtained ZnO, Al_2O_3 and ZnO-Al_2O_3 sols were coated onto the SAW resonators using a multi-spin-coating process (3 cycles), with a speed of 5000 rpm for 30 seconds for each cycle. The coated SAW resonators were immediately annealed in an oven at a temperature of 450 ^oC for one hour to obtain dense ZnO, Al_2O_3 and ZnO-Al_2O_3 layers. The ZnO, Al_2O_3 and ZnO-Al_2O_3 powders were also obtained by scrapping the prepared layers and were used for characterization.

The annealed resonators were connected to a cascaded amplifier with two BFT25A transistors and phase-shift circuits with two L-C networks to build the SAW sensor. Heaters made of Ni-Cr ribbon were mounted right below the resonators and were used to heat the resonators. The sensing performance of the SAW gas sensor was measured using a specially designed testing setup, as shown in Fig. 1. The sensor was put in a test chamber with a volume of 2 L. The temperature and relative humidity in the test chamber were maintained at 25 ^oC and 50% unless otherwise specified, controlled by an air conditioner and a humidity controller to minimized temperature and humidity variations. The testing gases (2 vol%, balanced with dry air) including H_2S, NH_3, CO, SO_2, CH_4, H_2 were injected into the chamber using a precision syringe. For example, with 0.1 ml H_2S gas injected, the concentration of the test gas in the chamber is 1 ppm. The response of the SAW sensor was defined as $\Delta f = f_s - f_0$, where f_s is the oscillating frequency of the sensor when exposed to the test gas, and f_0 is the oscillating frequency of the sensor in the ambient environment, respectively. The oscillating frequency of the SAW sensor was recorded using a frequency counter (HP 5385A). After the responses were recorded, the test gas was pumped out and pure air was filled in the chamber to allow the full recovery of the sensor. The time taken for the sensor to achieve 90% of the total frequency shift was defined as the response time in the response process.

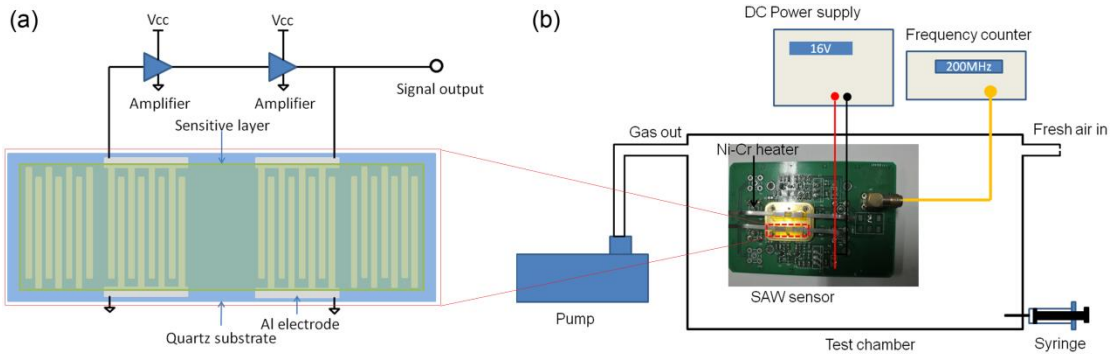

Fig. 1(a) The schematic diagram of a SAW sensor and (b) experimental setup for gas sensing measurement.

Electrical measurement of the sensing layers was conducted using a source meter (Keithley 2400). X-ray diffraction (XRD) were tested using Bruker AXS D8 ADVANCE X-ray diffractometer with a Cu Kα (λ = 1.5418 Å) radiation source, operating at 40 kV and 40 mA. Diffraction patterns were collected at a scanning rate of 2°/min and with a step size of 0.02°. Surface morphology and elemental compositions were obtained using a field-emission scanning electron microscope (SEM, FEI Inspect F) and an energy dispersive X-ray Spectroscopy (EDS). High angle annular dark field scanning transmission electron microscope (HAADF-STEM) and EDS mapping were used for microstructural analysis with a Double Cs-corrector FEI Titan Themis G2 60–300 microscope. Chemical states of the layers were analyzed using an X-ray photoelectron spectroscopy (XPS, Quantum 2000 Scanning ESCA Microprobe instrument) with a monochromatic Al Kα source (1486.6 eV). The S 2p spectra were deconvoluted using a commercially available data fitting program (XPSPEAK41 software). The surface area was evaluated based on the Brunauer–Emmett–Teller (BET) method using the instrument of ASAP-2020, with the adsorption branch in a relative pressure range from 0.01 to 1. The pore size distribution was derived from the adsorption branches of the isotherms using the Barrett–Joyner–Halenda (BJH) model.

3. Results and discussion

3.1. Characterization of prepared layers

The XRD patterns of prepared layers are shown in Fig. 2. For the pristine Al_2O_3 layer, two peaks at 45.9º and 66.6º observed are corresponding to the (400) and (440) planes of *γ*-alumina, indicating the prepared layer is consisted of *γ*-alumina. The XRD pattern of the pristine ZnO layer exhibits several peaks located at 31.8º, 34.4º, 36.3º, 47.5º, 56.6º, 62.8º and 68.0º, corresponding to ZnO (100), (002), (101), (102), (110), (103), and (200) crystal planes of Wurtzite ZnO. The Al_2O_3 and ZnO crystallite sizes in these pristine layers estimated using the Scherrer's equation are ~4 nm and ~30 nm, respectively.

The XRD pattern of the ZnO-Al_2O_3 layer shows both diffraction peaks of Al_2O_3 and ZnO. Hence, it demonstrates that *γ*-alumina and Wurtzite ZnO are co-existed in the as-prepared layer. In addition, the ZnO diffraction peaks of the ZnO-Al_2O_3 composite layer become wider, indicating that the ZnO crystallite size is smaller than that in the pristine ZnO layer. The ZnO crystallite size in the ZnO-Al_2O_3 layer is estimated to be ~23 nm based on the Scherrer's equation.

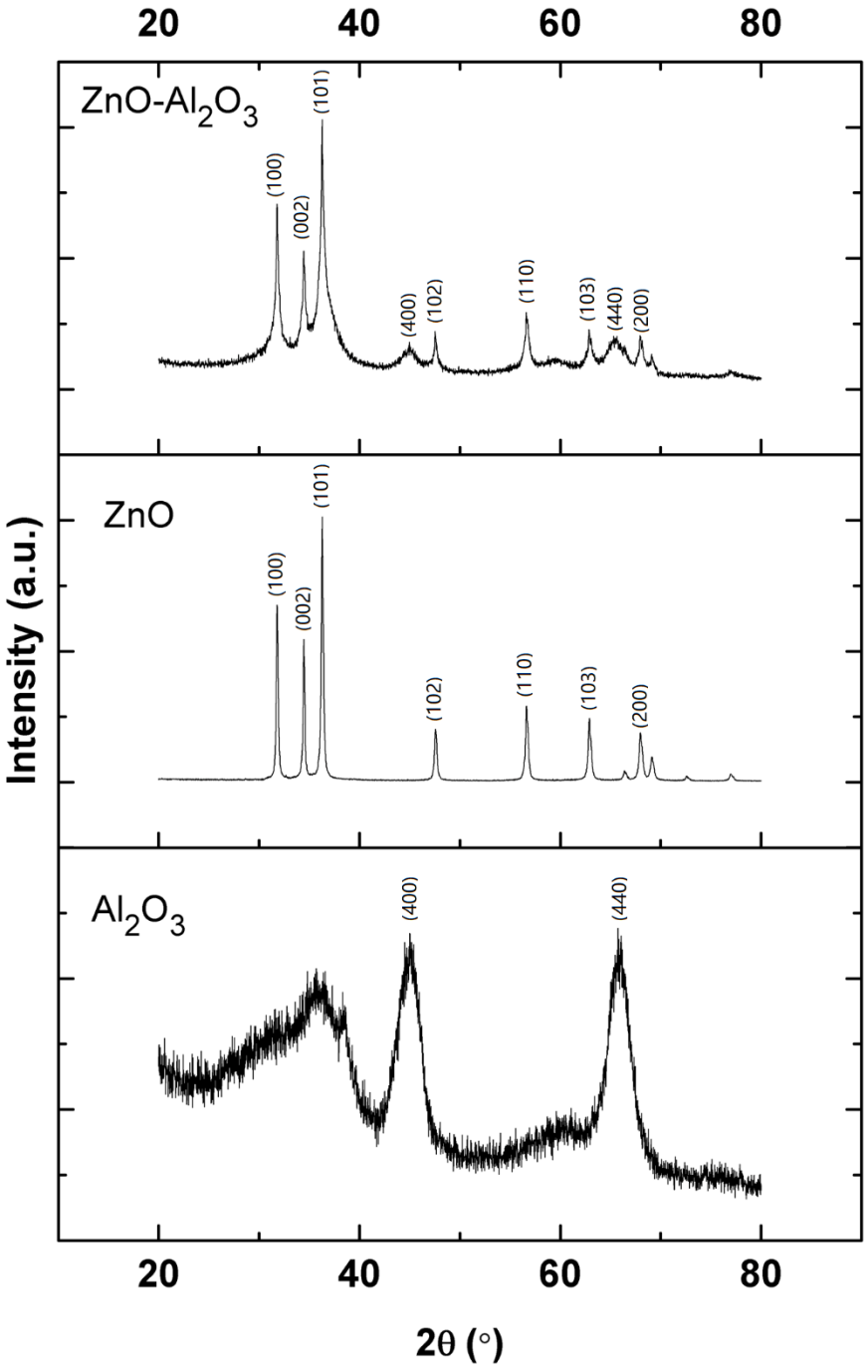

Fig. 2 XRD patterns of the Al_2O_3, ZnO, and ZnO-Al_2O_3 composite layers.

SEM images of surface morphologies for the pristine Al_2O_3, ZnO and ZnO-Al_2O_3 composite layers are presented in Fig. 3. The Al_2O_3 layer has a relatively rough surface,

which is composed of nanoparticles with an average diameter of ~20 nm. Pores with an average diameter of tens of nanometers can be found on the layer surface. The ZnO layer has a relatively dense and smooth surface where no apparent pores can be observed. The particles size of ZnO is not uniformly distributed, and the average size of the ZnO particles is ~30 nm. The composite ZnO-Al_2O_3 layer inherits the rough surface morphology of Al_2O_3 layer, and the average diameter of particles is ~20 nm. Pores are observed to be well-distributed on the surface of the ZnO-Al_2O_3 composite layer. The cross-sectional images of these three layers are shown in the insets, which indicate the thicknesses of these layers are all ~70 nm.

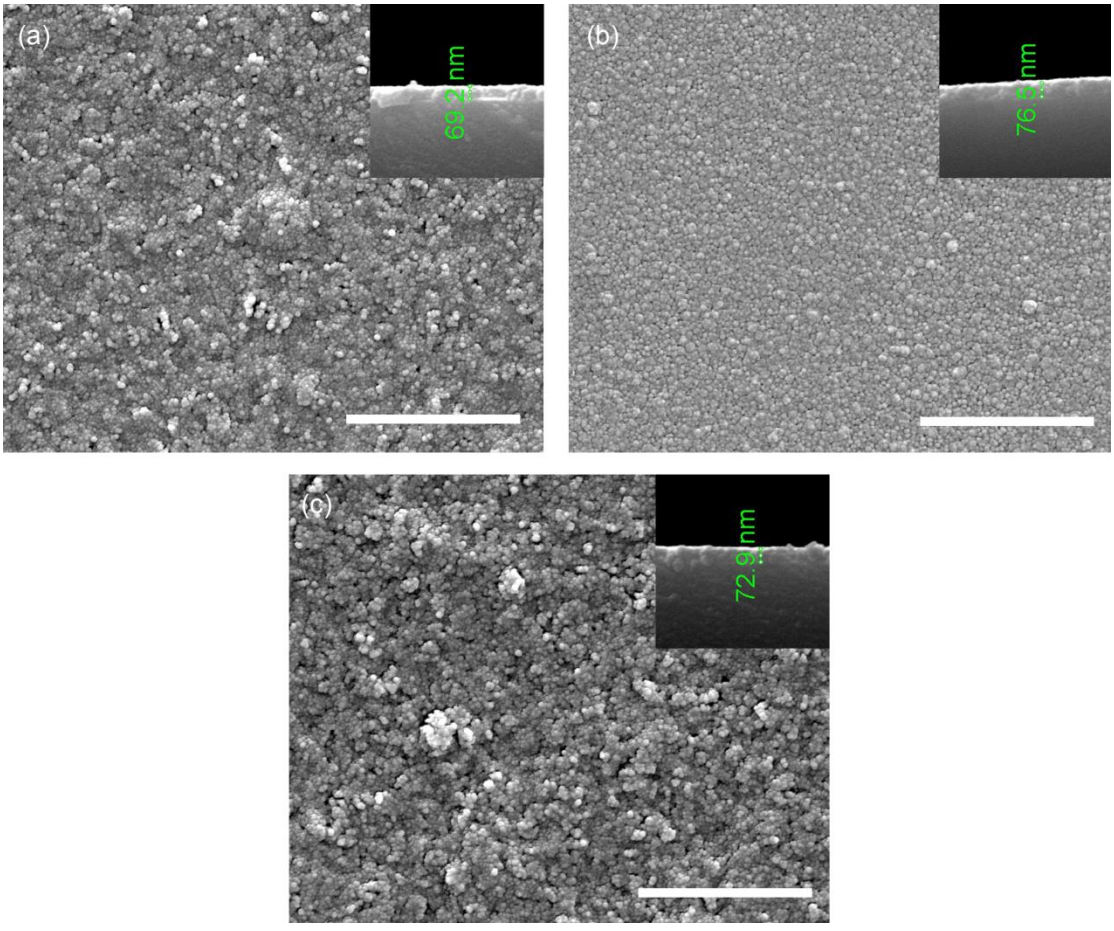

Fig. 3 SEM images of (a) Al_2O_3, (b) ZnO and (c) ZnO-Al_2O_3 layers. The scale bars in images are 1 μm. Inset images are the cross-sectional views of the layers.

Figs. 4(a) to 4(c) show the EDS results of the Al_2O_3, ZnO and Al_2O_3-ZnO layers after they were tested with H_2S gas. The signals of S element can be detected in the ZnO and Al_2O_3-ZnO spectra, while the spectrum of Al_2O_3 does not show any S signal. With this result, it can be speculated that ZnO may react with H_2S gas molecules while Al_2O_3 might not. Figs. 4(d) and 4(e) show the EDS spectra of H_2S tested ZnO and Al_2O_3-ZnO layers after they were heated further to 300 ^oC for 20 min in air. The signals of S element can no longer be observed in all these spectra, indicating that the layer may be recovered to its initial state after the heat-treatment process.

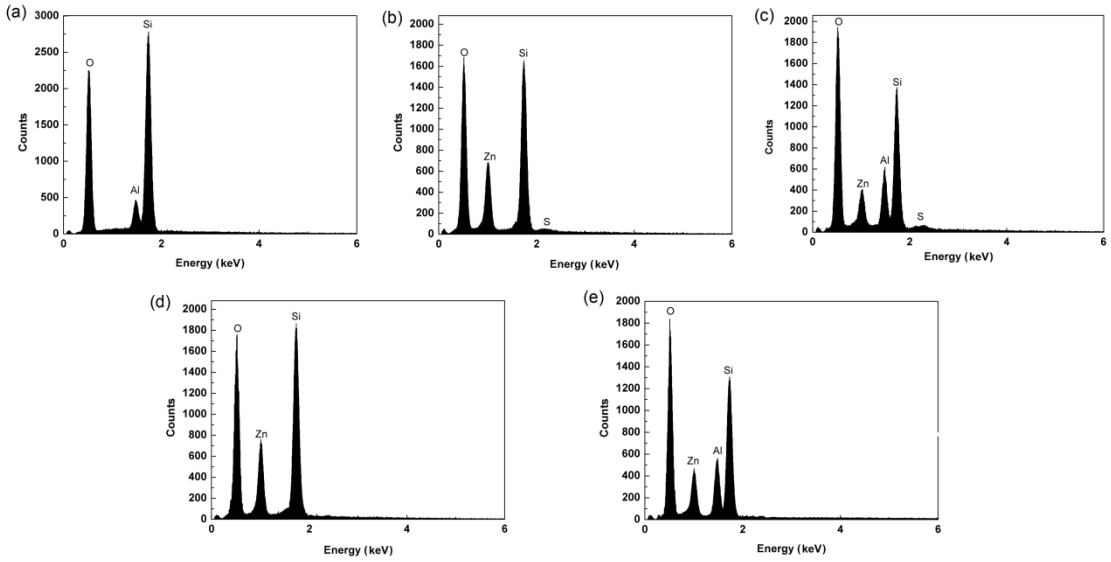

Fig. 4 EDS spectra of (a) Al_2O_3, (b) ZnO, (c) ZnO-Al_2O_3 layers after tested with H_2S gas and EDS spectra of H_2S-treated (d) ZnO, (e) ZnO-Al_2O_3 layers after heat-treatment.

Figs. 5(a) and 5(b) show the HAADF-STEM images of ZnO-Al_2O_3 powders obtained from the composite layer before and after tested with H_2S gas. The ZnO-Al_2O_3 materials clearly exhibit mesoporous structures with an average pore diameter of several nanometers. In addition, elemental mapping images of the ZnO-Al_2O_3 material after tested with H_2S gas (Figs. 5c to 5f) clearly present S element which is evenly

spread over the entire area of the material. These data confirm the sulfidization of ZnO-Al_2O_3 material when it is exposed to H_2S gas.

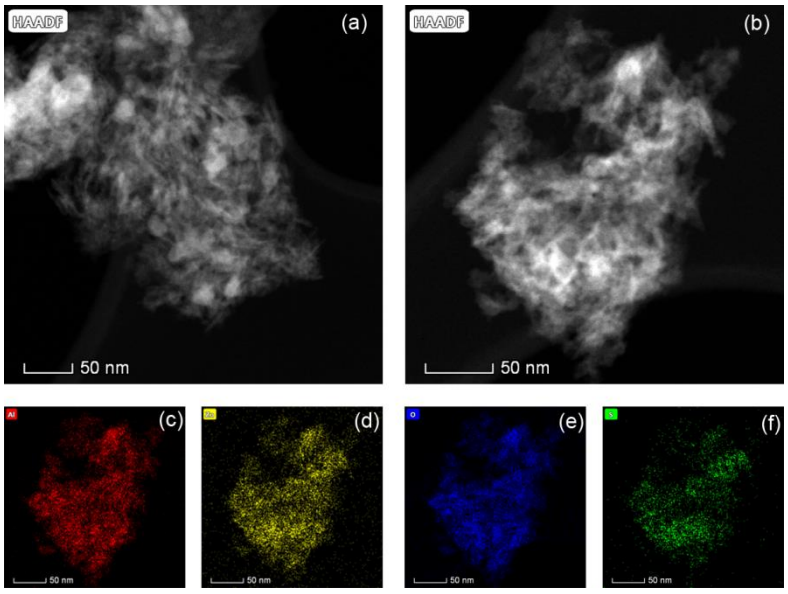

Fig. 5 HAADF-STEM images of ZnO-Al_2O_3 powders obtained from the layer (a) before and (b) after tested with H_2S gas. (c) Al, (d) Zn, (e) O, (f) S elemental mapping images of the ZnO-Al_2O_3 material after tested with H_2S gas.

To further investigate the valence state of different elements in the ZnO-Al_2O_3 materials before and after tested with H_2S gas, XPS survey spectra of the ZnO-Al_2O_3 materials in the range of 0-1200 eV were obtained and the result is shown in Fig. 6(a), in which peaks of Zn, Al, O, S and C are identified. The C 1s peak is due to surface contamination of carbon compounds (CO and hydrocarbons, etc.). Fig. 6(b) shows the high-resolution XPS curves in the region of 1016-1028 eV. There is a single normal peak at binding energy (BE) of 1022.5 eV for the ZnO-Al_2O_3 material before tested with H_2S, this can be assigned to the Zn $2p_{3/2}$ of ZnO [31,32]. After tested with H_2S, the BE of Zn $2p_{3/2}$ shifts from 1022.5 to 1021.8 eV, indicating that the conversion of ZnO to ZnS during the after tested with H_2S [32,33]. Fig. 6(c) shows there is a BE peak at 162 eV, which is the characteristic of the S 2p transition of sulfide [33-35]. Therefore,

it is concluded that the ZnO in the composite is chemically reacted with H_2S and turns to ZnS.

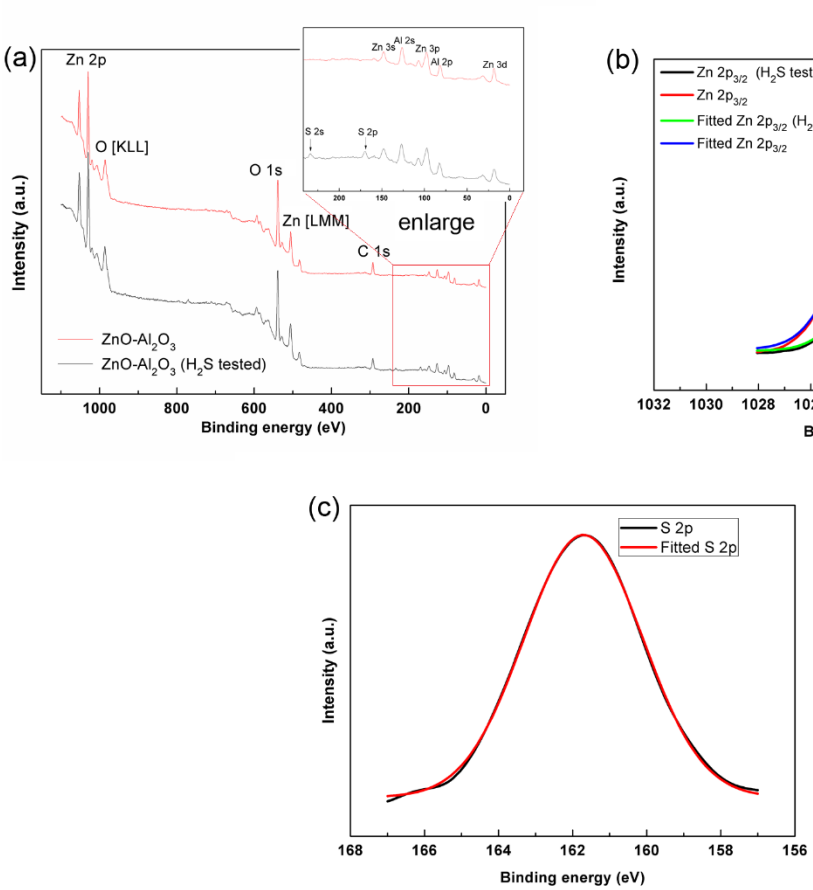

Fig. 6 (a) XPS spectra of the whole spectra (a), Zn $2p_{3/2}$ (b) and S 2p (c) narrow spectra for ZnO-Al_2O_3 materials before and after tested with H_2S gas.

The specific surface areas and pore distribution of the Al_2O_3, ZnO and ZnO-Al_2O_3 powders obtained from the deposited layers were immediately measured using the nitrogen adsorption method. The obtained results are shown in Fig. 7. The measured BET surface areas of Al_2O_3, ZnO and ZnO-Al_2O_3 materials are 267.8 m^2/g, 8.9 m^2/g and 125.1 m^2/g, respectively, as listed in Table 1. These results are consistent with those obtained from the SEM and STEM analysis, indicating that the Al_2O_3 and Al_2O_3-ZnO

materials are porous. In addition, Fig. 7(b) shows that the pore size ranges of the Al_2O_3 and Al_2O_3-ZnO materials are from 2 to 8 nm and 3 to 15 nm, respectively. The total pore volumes are 0.42 and 0.34 cm^3/g for Al_2O_3 and ZnO-Al_2O_3 materials, and the calculated average pore diameters are 4.9 nm and 8.6 nm, respectively. These mesopores are believed to be beneficial for the gas sensing application because they can act as the efficient paths for gas molecules to diffuse into the layers and providing more effective surfaces for the adsorption of and reaction with the gas molecules.

Fig. 7 also shows the N_2 adsorption and desorption isotherms and pore distribution of ZnO-Al_2O_3 material right after exposure with H_2S gas. Compared with that of the fresh ZnO-Al_2O_3, the BET surface areas of the H_2S exposed material are decreased to 107 m^2/g, and the total pore volume and average pore diameter are also decreased to 0.29 cm^3/g and 8.1 nm, respectively, as listed in Table 1. These results indicate that the reaction between the ZnO-Al_2O_3 material and H_2S gas molecules leads to a decrease of the pore size and total pore volume in the material. This could indicate clearly the H_2S gas molecules have been adsorbed onto and reacted with their pore surfaces.

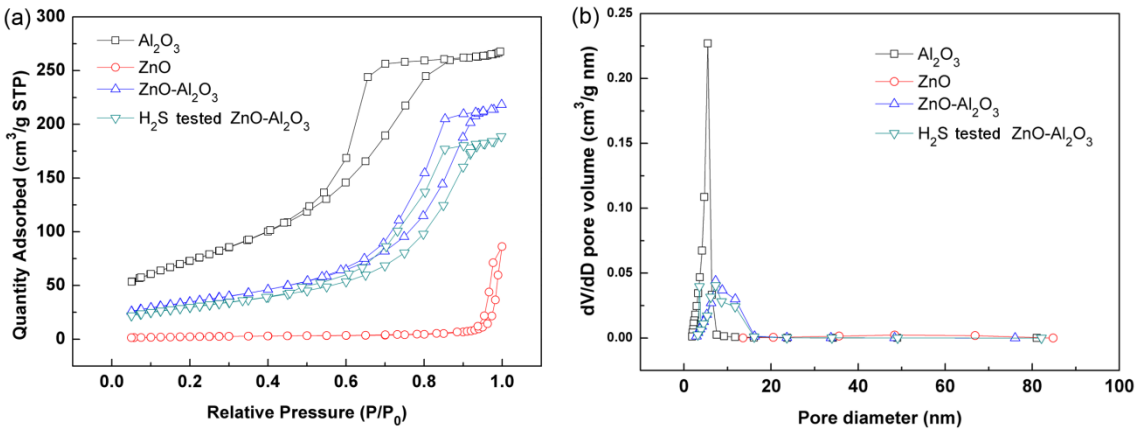

Fig. 7 (a) N_2 adsorption and desorption isotherms and (b) pore distributions of the Al_2O_3, ZnO and ZnO-Al_2O_3 materials before and after tested with H_2S gas.

Table 1 Surface areas, pore volumes and average diameters of the Al_2O_3, ZnO powders and ZnO-Al_2O_3 powders before and after tested with H_2S gas.

Material	BET surface area (m^2/g)	Total pore volume (cm^3/g)	Average pore diameter (nm)
Al_2O_3	267.8	0.42	4.9
ZnO	8.9	0.13	50.6
ZnO-Al_2O_3	125.1	0.34	8.6
H_2S-tested ZnO-Al_2O_3	107	0.29	8.1

3.2. Gas Sensing performance and the sensing mechanism

The SAW sensors coated with the pristine ZnO and Al_2O_3 layers were firstly tested at room temperature, and the results are shown in Fig. 8(a). The sensor with the Al_2O_3 layer shows no apparent responses to the H_2S gas, while the sensor with the ZnO layer shows a negative response of ~-350 Hz when it is exposed to the 1 ppm H_2S for the first time. This result indicates that the Al_2O_3 has a relatively poor affinity for the H_2S gas, while there are some changes on the ZnO layer since ZnO has a good affinity for H_2S [23-26]. When the first response of the sensor with the ZnO layer became stable, the sensor was then exposed to the air to allow its full recovery. However, as shown in the 1st cycle in Fig. 8(a), the working frequency of the sensor has its new baseline which is decreased. Besides, with continuously exposed this ZnO layer SAW sensor to 1 ppm H_2S gas for another 2 cycles (the 2nd and 3rd cycles in Fig. 8(a)), the response becomes weaker and the baseline keeps decreasing. This result indicates that the sensor cannot be recovered to its initial state at room temperature. In other words, there is an irreversible reaction occurring between the ZnO layer and H_2S gas when the sensor is exposed to H_2S gas at room temperature.

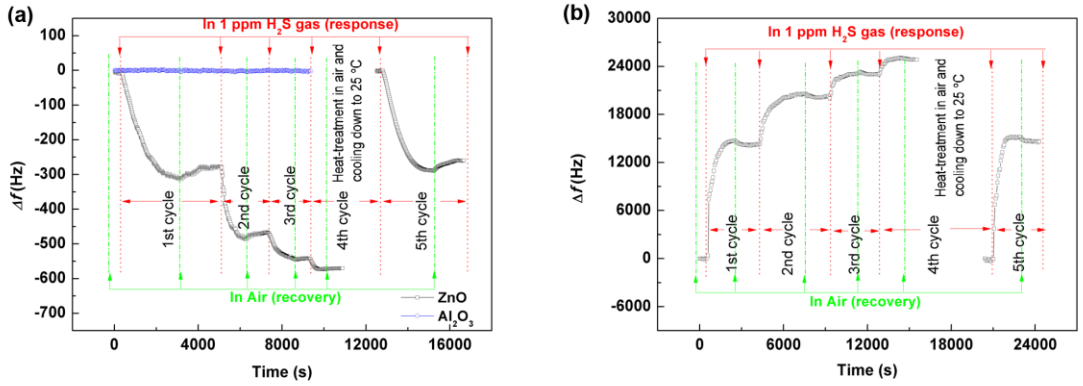

Fig. 8 Five dynamic response and recovery cycles of the sensors with (a) pristine ZnO layer and Al_2O_3 layer and (b) ZnO-Al_2O_3 layer to 1 ppm H_2S gas. The red arrows in figures indicate where the H_2S gas was introduced in the test chamber while the green arrows indicate where the H_2S gas was evacuated and fresh air was introduced to allow the recovery of the sensors. Full recovery of the sensors with ZnO and ZnO-Al_2O_3 layers can not be achieved in prior three cycles, whereas the full recovery was achieved in the 4^{th} cycle by heating the sensitive layers at 300 °C in the ambient environment for 20 min and then cooled down to 25 °C.

Previous studies have revealed that H_2S can spontaneously react with ZnO based on the following formula: [23, 27-29]

$$ZnO+H_2S(ads) \rightarrow ZnS+H_2O \quad (1)$$

This reaction has a negative enthalpy [23], indicating that the reaction between ZnO and H_2S is an irreversible and exothermic process at room temperature. Therefore, this spontaneous reaction between ZnO and H_2S could be the main reason for the poor recovery of frequency signal for the sensor operated at room temperature. To verify this, we have done EDS analysis of the ZnO layer after tested with H_2S gas. Result illustrated in Fig. 4 clearly indicates that S element is presented on the ZnO layer after it is exposed to the H_2S gas. This can confirm our assumption.

Although the reaction (1) is irreversible at room temperature, previous studies have revealed that it may become reversible when the sensing temperature is increased to 300 ^{o}C or above [36]. We have further heat-treated the H_2S-tested ZnO layer at 300 ^{o}C for 20 min and then allow it to cool down naturally to room temperature, and then recorded the sensor's response to 1 ppm H_2S gas. Results shown in the 4th and 5th cycles in Fig. 8(a) clearly reveal that the sensor with the heat-treated H_2S-tested ZnO layer has a similar baseline and also similar response to 1 ppm H_2S gas as those of the original sensor. Results indicate that the recovery of the layer can be achieved at a high temperature of 300 ^{o}C. This can be further confirmed by the EDS results (Fig. 4) of the heat-treated H_2S-tested ZnO layer because there are no S signals detected.

The H_2S sensing performance of the sensor with the ZnO-Al_2O_3 composite layer was investigated. As shown in Fig. 8(b), compared with the results obtained from the sensor with ZnO layer, this sensor using the nanocomposite layer showed different sensing performance to H_2S gases. The response of the sensor to 1 ppm H_2S was positive and as high as ~15 kHz when the sensor was used for the first time. However, similar as the sensor with the ZnO layer, this sensor also had a poor recovery property and its baseline was increased gradually when the sensor was repeatedly exposed to 1 ppm H_2S at room temperature as shown in the 1st to 3rd cycles in Fig. 8(b). By checking the XPS and EDS results of the ZnO-Al_2O_3 layer after tested with H_2S, it can also be confirmed that the reaction (1) has occurred on the ZnO-Al_2O_3 composite layer. A heat-treatment at ambient environment has also led to the full recovery of the sensor, and the results are shown in the 4th and 5th cycles in Fig. 8(b).

As discussed above, we can confirm that both the responses of the sensors with ZnO and ZnO-Al_2O_3 layers are caused due to the reaction (1). However, their sensing results for H_2S gas are totally different. The sensor with ZnO layer shows negative

responses while the sensor with ZnO-Al_2O_3 layer exhibits much stronger positive responses. It is well known that three key property changes of the sensing layers can contribute to the total responses of SAW sensors, i.e. the changes of mass (mass loading effect), elastic modulus (elastic loading effect) and electrical conductivity (electrical loading effect) [18-20,34]. Table 2 summarizes the influences of these different effects on the working frequency (*f*) and response (frequency shift, Δf) of a SAW gas sensor.

Table 2 Effects of mass, electrical and elastic loading on working frequencies and responses. '↑'indicates increase, '↓' indicates decrease.

Loading	Working frequency (*f*)	Response (frequency shift, Δf)
Mass↑	↓	Negative
Mass↓	↑	Positive
Elastic↑ (modulus ↑)	↑	Positive
Elastic↓ (modulus ↓)	↓	Negative
Electrical↑ (Conductivity↑)	↓	Negative
Electrical↓ (Conductivity↓)	↑	Positive

To investigate the contribution of electrical loading effect to the responses of the sensors to H_2S gas, the conductivity values of the ZnO and ZnO-Al_2O_3 layers on SAW resonators were recorded using a 4-probe testing method with a Keithley 2400 source meter at room temperature. As shown in Fig. 9, the conductivity values of both the ZnO and ZnO-Al_2O_3 layers are increased from 4.45×10^{-5} S/cm and 7.12×10^{-6} S/cm to

8.22×10^{-4} S/cm and 9.89×10^{-5} S/cm, respectively, when these two layer coated sensors were put inside the H_2S gas with a concentration of 1 ppm for the first time. In addition, the conductivity values cannot be fully recovered to their initial values after the sensing test, indicating the poor recovery property of both the ZnO and ZnO-Al_2O_3 coated SAW devices toward H_2S gas at room temperature.

The relationship between the response (Δf) and the electric loading is given below [37],

$$\Delta f = -f_0 \times \frac{K^2}{2} \times \Delta\left(\frac{1}{1+\left(\frac{v_0 c_s}{\sigma_s}\right)^2}\right) \quad (2)$$

where f_0 (= ~200 MHz) is the resonant working frequency of the ST-cut quartz SAW resonator, V_0 (= 3158 m/s) is the unperturbed SAW velocity on the SAW resonator, K^2 (= 0.0011) is the electromechanical coupling coefficient for ST-cut quartz substrate, C_s (= ~0.5 pF/cm) is the capacitance of the SAW resonator per unit length, and σ_s is the sheet conductivity of the sensing film. However, based on the measured σ_s values, the calculated values of Δf contributed from the electrical loading, are all far less than the measured responses of the sensors. Therefore, it can be concluded these measured responses of the sensors are must be from effects of mass and elastic loadings.

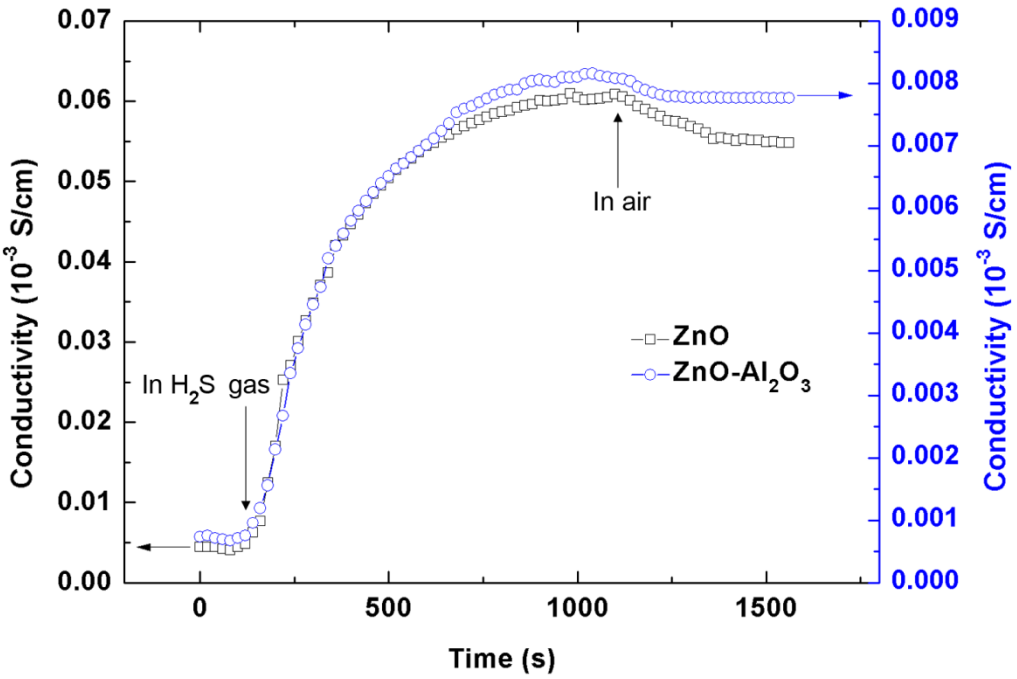

Fig. 9. Dynamic conductivity changes of the ZnO layer and ZnO-Al_2O_3 layer during their exposure to 1 ppm H_2S gas for the first time. The arrows in figures indicate where the H_2S gas was introduced in the test chamber and where the H_2S gas was evacuated and fresh air was introduced to allow the recovery of the sensors. Full recovery of the conductivity of ZnO and ZnO-Al_2O_3 layers can not be achieved.

When exposed to H_2S gas, an increase of mass of these layers can be expected because of the higher molar mass of the newly formed ZnS on the surface of ZnO nanoparticles, as illustrated in Fig. 10. Besides, the elastic moduli of these layers may be also increased, since the newly formed ZnS also has a lower density compared with that of original ZnO. Therefore, with this heavier and lower-density ZnS layer covered on the surfaces of ZnO nanoparticles, the volumes of the original ZnO nano-particles will be increased and the pore sizes in the layer will be decreased as illustrated in Fig.

10. The decreased pore size would lead to a decrease of the total pore volume of the layer, as confirmed by the N_2 sorption result as shown in Fig. 7 and also listed in Table 1. The significant decreases of the pore diameters and the total pore volumes in the layer would result in increases of the elastic moduli of the layers [18-20]. Clearly the increase of the mass and the elastic moduli of the layers caused by the formation of ZnS layer would lead to a negative and a positive response of the SAW sensor, respectively, as listed in Table 2.

Based on the discussions above, both the mass and elastic loading effects may contribute to the responses of the sensor. However, the negative response of the sensor coated with ZnO layer is mainly caused by the mass loading effect, whereas the positive responses of the sensor with the ZnO-Al_2O_3 layer is mainly contributed by the elastic loading effect. The differences between the sensing performances and mechanisms of these two sensors are mainly caused by the different microstructures of the sensing layer materials. Results from SEM, STEM and N_2 sorption analysis have revealed that the ZnO-Al_2O_3 layer has a mesoporous structure and a rough surface, whereas the ZnO layer is relatively dense and smooth. When the ZnO layer is exposed to the H_2S gas molecules, these molecules will react mainly with the ZnO particles on the layer surfaces as shown in Fig. 10 (upper panel). In this case, the mass of the ZnO layer will be increased but the elastic modulus of the ZnO layer will not be apparently changed, thus leading to the negative responses of the sensor.

Whereas when the porous ZnO-Al_2O_3 layer is exposed to H_2S gas, a large amount of H_2S molecules can enter deeply inside the layer through the porous structures and then are adsorbed on and react with ZnO nano-particles inside the porous structures of layer, thus leading to the significant expansion of these ZnO nano-particles, as shown in Fig. 10 (lower panel). This expansion leads to significant decreases of both the pore

sizes and the total pore volumes of the layer, as confirmed by the N_2 sorption results shown in Fig. 7 and listed in Table 1. Consequently, the contribution of elastic loading effect toward the sensing responses has been dramatically enhanced whereas there is a relatively less effect from the mass loading effect. These phenomena will result in a positive response of the sensor, and this effect is much more significant only when the sensing layer is highly porous and reactive as the ZnO-Al_2O_3 layer in this study.

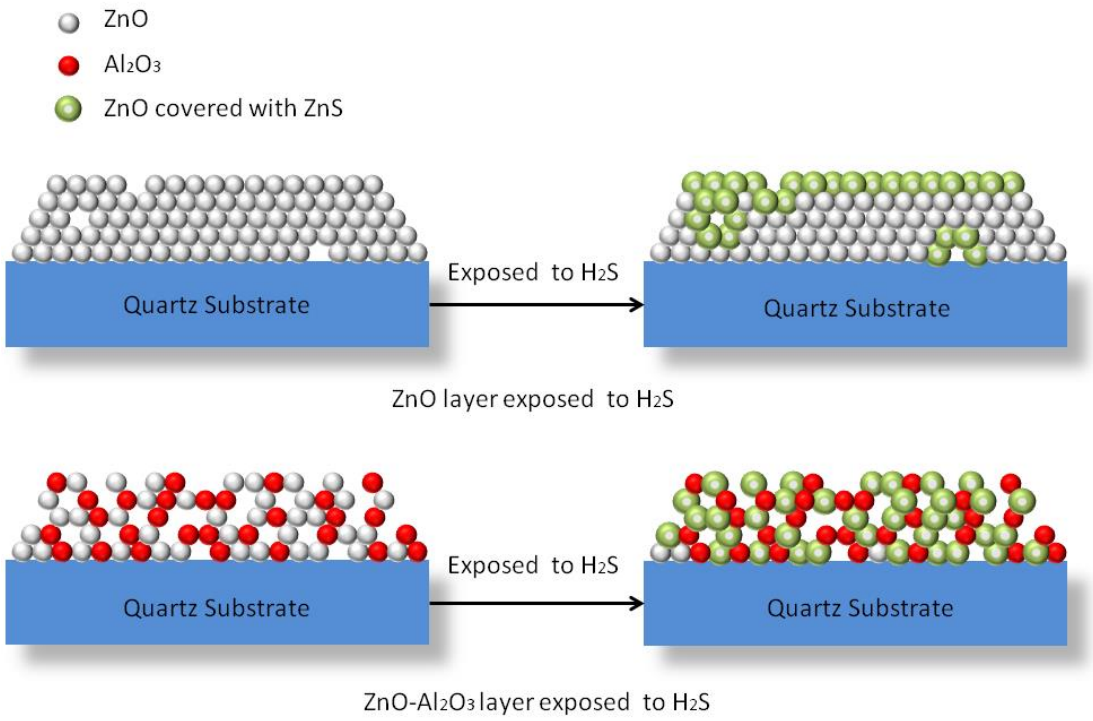

Fig. 10 Proposed H_2S sensing mechanism of the sensors with the coated ZnO layer and ZnO-Al_2O_3 layer, respectively.

For the following measurements, we will use the sensor with ZnO-Al_2O_3 layer to study its sensing performance. During the measurements, the sensitive layer was heated to 300 ^oC in the ambient environment for 20 min and then cooled down naturally to 25 ^oC after each response process to H_2S gas in order to make sure the full recovery of the sensor. Fig. 11 presents the dynamic sensing performance of this sensor toward H_2S gas with concentrations changing from 10 ppb to 20 ppm. As is shown, the sensor has a

response of 0.5 kHz to 10 ppb H_2S gas, and the response can reach up to 38 kHz when the concentration is 20 ppm. The response of the sensor increases significantly with the gas concentration at a low H_2S concentration range (< 1ppm), however, it becomes gradually saturated when the H_2S concentration is higher than 4 ppm. This saturation may be due to the limited ZnO surfaces in the nanocomposite layer, which leads to saturated amount of ZnS formed. The response time also increases with the gas concentration, and it reaches at ~830 s when the H_2S has a concentration of 20 ppm (Fig. 11(b)).

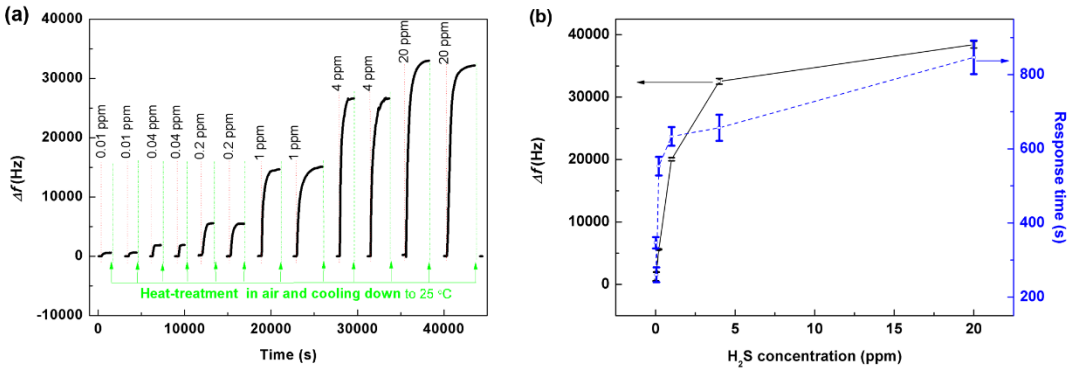

Fig. 11 (a) Dynamic responses of the sensor with the ZnO-Al_2O_3 layer to 0.01-20 ppm H_2S gas. The sensitive layer was heated at 300 °C in the ambient environment for 20 min and then cooled down to 25 °C after each testing process to allow the full recovery of the sensor; (b) The response and response times as functions of H_2S gas concentration.

The selectivity of the sensor was further investigated, and the results are shown in Fig. 12(a). Clearly the sensor has no apparent responses to 10 ppm of CH_4, H_2, CO, and ethanol gases, while it shows slight positive responses to NH_3 and SO_2 gases. These slightly positive responses may be caused by the adsorbed H_2O molecules on the layer, which worked as the active sites for capturing SO_2 and NH_3 since these gases have a high solubility in H_2O. Our previous report [38] has revealed that these captured SO_2

and NH_3 can catalyze the condensation reaction between the hydrophilic groups on the sensitive film. The condensation would lead to an increase of the elastic modulus, which causes positive responses. However, the responses to SO_2 and NH_3 are much weaker than that to H_2S, as shown in Fig. 12(a). This result indicates that the sensor has a good selectivity to H_2S gas. This is due to the distinct reaction (1) between ZnO and H_2S gas.

Good stability is another critical parameter for a practical sensor. Therefore, the stability of the sensing performance was further investigated by conducting the sensing test every 10 days within a 90 day period. As shown in Fig. 12(b), the sensor shows the similar responses to 0.2 ppm, 1 ppm and 4 ppm H_2S, respectively, in the 10 different tests within 90 days, indicating its good stability.

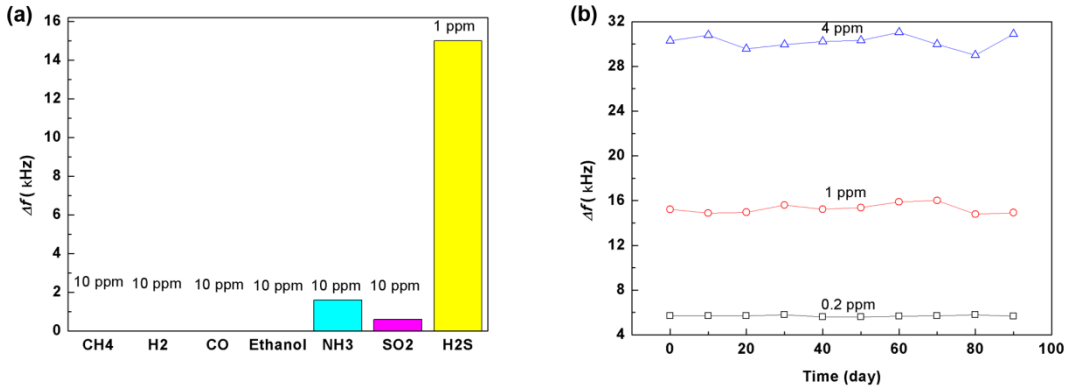

Fig. 12 (a) The response of the sensor with ZnO-Al_2O_3 layer to 10 ppm CH_4, H_2, CO, ethanol, NH_3, SO_2 and 1 ppm H_2S gases; (b) The responses of the sensor with ZnO-Al_2O_3 layer to 0.2, 1 and 4 ppm H_2S gas within 90 days.

Humidity resistance is also a critical parameter for a good gas sensor. The influence of the humid condition on the H_2S response of the sensor was measured under RH of 10%, 50% and 90%. Fig. 13 shows that the baseline of the sensor has negative shifts of -3.3 kHz and -9.8 kHz, when the RH increases from 10% to 50% and 90%, respectively.

These shifts of baseline indicate that more H_2O molecules were adsorbed on the layer at higher RH values, which leads to an increased weight of the layer. Thus, this sensor may also be used as a sensitive humidity sensor. Fig. 13 also presents that the sensor's response to 1 ppm H_2S has a slight decrease from 17.2 kHz to 13.2 kHz with the increase of the relative humidity from 10% to 90%. This result may be caused by the increased amount of H_2O molecules occupying the ZnO surface in the porous film at higher RH, which thus leads to decreased active ZnO sites for the adsorption of H_2S. With this result, it can be confirmed that this sensor can be used for H_2S detection at different environments with RH value ranging from 10% to 90%.

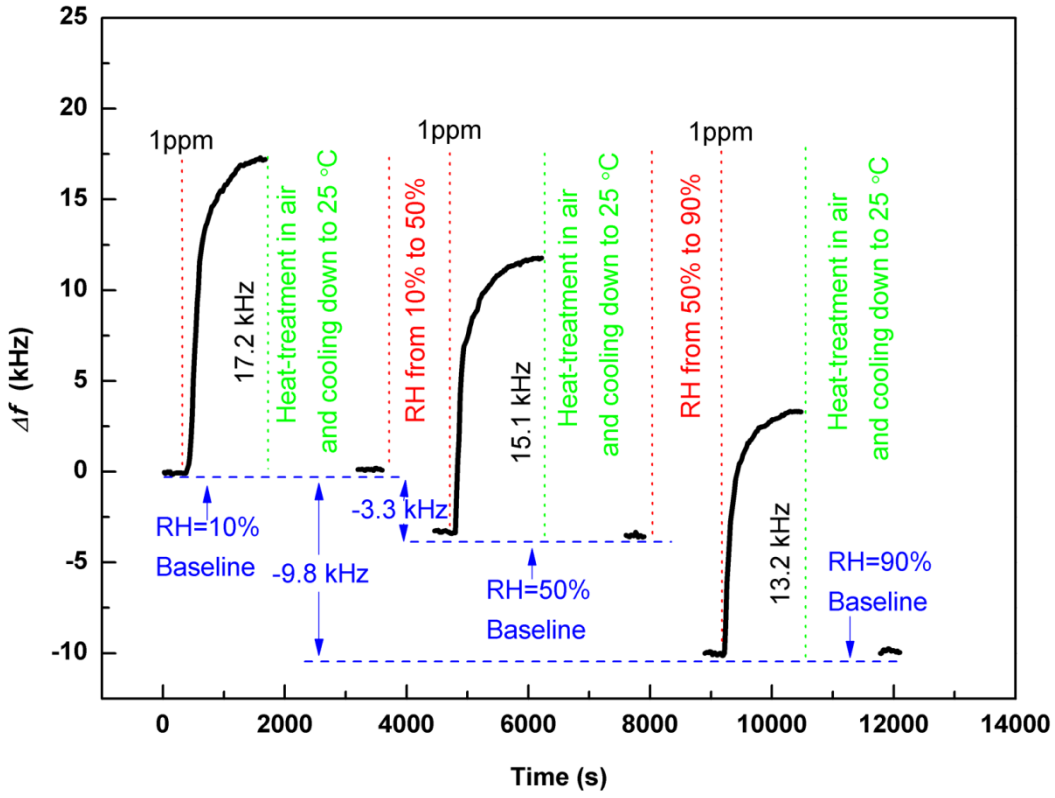

Fig. 13 Dynamic responses of the sensor with the ZnO-Al_2O_3 layer to 1 ppm H_2S gas under environments with different RH. The sensor was heated at 300 °C in the ambient environment for 20 min and then cooled down to 25 °C after each testing process to allow the full recovery of the sensor. The shifts of baseline can be observed when RH changes.

Conclusions

In this paper, the H_2S gas sensing performance of quartz SAW sensors with pristine ZnO, Al_2O_3 and ZnO-Al_2O_3 composite layers were investigated and compared. It is found that the sensor coated with ZnO-Al_2O_3 composite layer has the highest sensitivity of 15 kHz/ppm, and the responses of the sensors are mainly caused by the formation of ZnS through the reactions between the adsorbed H_2S and ZnO. In addition, the different morphologies and microstructures of ZnO and ZnO-Al_2O_3 layers results in different responses of the sensors. The porous structure of ZnO-Al_2O_3 layer is beneficial for the adsorption of H_2S and elastic loading effect of the SAW sensor, which leads to a more significant response, with excellent stability, selectivity and humidity resistance to H_2S gas.

Acknowledgements

This work was supported by the Fundamental Research Funds for the Central Universities (A0920502051904-67, A0920502051903-42), the Scientific Research Foundation of SWJTU (A1920502051907-2-032), the National Natural Science Foundation of China (11805158, 61178018) and the NSAF Joint Foundation of China (U1630126 and U1230124), the UK Engineering and Physical Sciences Research Council (EPSRC) grants EP/P018998/1, Newton Mobility Grant (IE161019) through Royal Society and the National Natural Science Foundation of China.

Declaration of interests

The authors declare no conflicts of interests.

Reference

[1] T.L. Guidotti, Hydrogen sulfide: advances in understanding human toxicity, Int. J. Toxicol. 29 (2010) 569-581.

[2] T.H. Milby, R.C. Baselt, Hydrogen sulfide poisoning: clarification of some controversial issues, Am. J. Ind. Med. 35 (1999) 192-195.

[3] B. Tvedt, A. Edland, K. Skyberg, O. Forberg, Delayed neuropsychiatric sequelae after acute hydrogen sulfide poisoning: affection of motor function, memory, vision and hearing, Acta Neurol. Sca. 84 (1991) 348-351.

[4] R.G. Hendrickson, A. Chang, R.J. Hamilton. Co-worker fatalities from hydrogen sulfide, Am. J. Ind. Med. 45 (2004) 346-350.

[5] M.G. Costigan, Hydrogen sulfide: UK occupational exposure limits, Occup. Environ. Med. 60 (2003) 308-312.

[6] A.A. Khan, M.M. Schuler, M.G. Prior, S. Yong, R.W. Coppock, L.Z. Florence, L.E. Lillie, Effects of hydrogen sulfide exposure on lung mitochondrial respiratory chain enzymes in rats, Toxicology and applied pharmacology 103 (1990) 482-490.

[7] G. Ahlborg, Hydrogen sulfide poisoning in shale oil industry, Arch. Indust. Hyg. & Occupational Med. 3 (1951) 247-66.

[8] O. Yassine, O. Shekhah, A.H. Assen, Y. Belmabkhout, K.N. Salama, M. Eddaoudi, H_2S Sensors: Fumarate-Based fcu-MOF Thin Layer Grown on a Capacitive Interdigitated Electrode, Angew. Chem. Inter. 55 (2016) 15879-15883.

[9] T.L. Guidotti, Occupational exposure to hydrogen sulfide in the sour gas industry: some unresolved issues, Int. Arch. Occ. Env. Hea. 66 (1994) 153-160.

[10] D. Li, X. Zu, D. Ao, Q. Tang, Y. Fu, Y. Guo, K. Bilawal, M.B. Faheem, L. Li, S. Li, Y. Tang, High humidity enhanced surface acoustic wave (SAW) H_2S sensors based on sol–gel CuO layers. Sens. Actuators B 294 (2019) 55-61.

[11] W. Luo, J. Deng, Q. Fu, D. Zhou, Y. Hu, S. Gong, Z. Zheng, Nanocrystalline SnO_2 layer prepared by the aqueous sol–gel method and its application as sensing layers of the resistance and SAW H_2S sensor, Sens. Actuators B 217 (2015) 119-128.

[12] X. Liu, W. Wang, Y. Zhang, Y. Pan, Y. Liang, J. Li, Enhanced Sensitivity of a Hydrogen Sulfide Sensor Based on Surface Acoustic Waves at Room Temperature, Sensors 18 (2018) 3796.

[13] M. Asad, M.H. Sheikhi, Surface acoustic wave based H_2S gas sensors incorporating sensitive layers of single wall carbon nanotubes decorated with Cu nanoparticles, Sens. Actuators B 198 (2014) 134-141.

[14] X. Wang, W. Wang, H. Li, C. Fu, Y. Ke, S. He, Development of a SnO_2/CuO-coated surface acoustic wave-based H_2S sensor with switch-like response and recovery, Sens. Actuators B 169 (2012) 10-16.

[15] J.D. Galipeau, R.S. Falconer, J.F. Vetelino, J.J. Caron, E.L. Wittman, M.G. Schweyer, J.C. Andle, Theory, design and operation of a surface acoustic wave hydrogen sulfide microsensor, Sens. Actuators B 24 (1995) 49-53.

[16] W. Luo, Q. Fu, D. Zhou, H. Liu, G. Yan, A surface acoustic wave H_2S gas sensor employing nanocrystalline SnO_2 thin layer, Sens. Actuators B 176 (2013) 746-752.

[17] X.F. Yan, D.M. Li, C.C. Hou, X. Wang, W. Zhou, M. Liu, T.C. Ye, Comparison of response towards NO_2 and H_2S of PPy and PPy/TiO_2 as SAW sensitive layers, Sens. Actuators B 161 (2012) 329-333.

[18] V.B. Raj, A.T. Nimal, Y. Parmar, M.U. Sharma, V. Gupta, Investigations on the origin of mass and elastic loading in the time varying distinct response of ZnO SAW ammonia sensor, Sens. Actuators B 166 (2012) 576-585.

[19] V.B. Raj, A.T. Nimal, Y. Parmar, M.U. Sharma, K. Sreenvias, V. Gupta, Cross-sensitivity and selectivity studies on ZnO surface acoustic wave ammonia sensor, Sens.

Actuators B 147 (2010) 517-524.

[20] V.B. Raj, H. Singh, A.T. Nimal, M. Tomar, M.U. Sharma, V. Gupta, Origin and role of elasticity in the enhanced DMMP detection by ZnO/SAW sensor, Sens. Actuators B 207 (2015) 375-382.

[21] J. Devkota, P. Ohodnicki, D. Greve, SAW sensors for chemical vapors and gases, Sensors 17 (2017) 801.

[22] V.B. Raj, A.T. Nimal, M. Tomar, M.U. Sharma, V. Gupta, Novel scheme to improve SnO_2/SAW sensor performance for NO_2 gas by detuning the sensor oscillator frequency, Sens. Actuators B 220 (2015) 154-161.

[23] G. Liu, Z.H. Huang, F. Kang, Preparation of ZnO/SiO_2 gel composites and their performance of H_2S removal at room temperature, J. Hazard. Mater. 215 (2012) 166-172.

[24] C. Yang, S. Yang, H. Fan, Y. Wang, J. Shangguan, Tuning the ZnO-activated carbon interaction through nitrogen modification for enhancing the H_2S removal capacity. J. Colloid Inter. Sci. 555 (2019) 548-557.

[25] K.Y. Chen, Y.Y. Chen, W.C.J. Wei, 3D printed ZnO absorbent for desulfurization of syngas fuel, 2017 IEEE/SICE International Symposium on System Integration (SII), IEEE 2017 115-120.

[26] Z.S. Hosseini, A. Mortezaali, Room temperature H_2S gas sensor based on rather aligned ZnO nanorods with flower-like structures, Sens. Actuators B 207 (2015) 865-871.

[27] G.K. Mani, J.B.B. Rayappan, Selective recognition of hydrogen sulfide using template and catalyst free grown ZnO nanorods, RSC Adv. 5 (2015) 54952-54962.

[28] G. Qi, L. Zhang, Z. Yuan, Improved H_2S gas sensing properties of ZnO nanorods decorated by a several nm ZnS thin layer, Phys. Chem. Chem. Phys.16 (2014) 13434-

527 13439.
528 [29] Z. Liu, T. Fan, D. Zhang, X.Gong, J. Xu, Hierarchically porous ZnO with high
529 sensitivity and selectivity to H_2S derived from biotemplates, Sens. Actuators B 136
530 (2009) 499-509.
531 [30] Y.L. Tang, Z.J. Li, J.Y. Ma, Y.J. Guo, Y.Q. Fu, X.T. Zu, Ammonia gas sensors based
532 on ZnO/SiO_2 bi-layer nanolayers on ST-cut quartz surface acoustic wave devices, Sens.
533 Actuators B 201 (2014) 114-121.
534 [31] S.W. Gaarenstroom, N. Winograd, Initial and final state effects in the ESCA spectra
535 of cadmium and silver oxides, J. Chem. Phys. 67 (1977) 3500-3506.
536 [32] S. Chaturvedi, J.A. Rodriguez, J. Hrbek, Reaction of S-2 with ZnO and Cu/ZnO
537 surfaces: photoemission and molecular orbital studies, J. Phys. Chem. B 101(1997)
538 10860-10869.
539 [33] J.A. Rodriguez, T. Jirsak, S. Chaturvedi, J. Hrbek, The interaction of H_2S and S-2
540 with Cs and Cs/ZnO surfaces: photoemission and molecular-orbital studies, Surf. Sci.
541 407 (1998) 171-188.
542 [34] L. Liu, R. Xie, L. Yang, D. Xiao, J. Zhu, Synthesis, structural, and optical
543 properties of core/shell ZnS:Fe/ZnS nanocrystals, Phys. Status Solidi A-Appl. Mater.
544 208 (2011) 863-867.
545 [35] X. Wang, T. Sun, J. Yang, L. Zhao, J. Jia, Low-temperature H_2S removal from gas
546 streams with SBA-15 supported ZnO nanoparticles, Chem. Eng. J. 142 (2008) 48-55.
547 [36] D. Wang, X. Chu, M. Gong, Hydrothermal growth of ZnO nanoscrewdrivers and
548 their gas sensing properties, Nanotechnology 18 (2007) 185601.
549 [37] A.J. Ricco, S.J. Martin, T.E. Zipperian, Surface acoustic wave gas sensor based on
550 layer conductivity changes, Sens. Actuators 8 (1985) 319–333.
551 [38] Y. Tang, D. Ao, W. Li, X. Zu, S. Li, Y. Fu, NH_3 sensing property and mechanisms

552 of quartz surface acoustic wave sensors deposited with SiO_2, TiO_2, and SiO_2-TiO_2
553 composite layers, Sens. Actuators B 254 (2018) 1165-1173.